Cover Letter

Mathematical modeling of the impact of vehicles on water-saturated soil

Igor Ratnere, Ph.D.

Dear Editors-in-Chief,

please find the enclosed manuscript "Mathematical modeling of the impact of vehicles on water-saturated soil" which we are submitting for exclusive consideration for publication in Computers & Geosciences. We confirm that the submission follows all the requirements and includes all the items of the submission checklist.

The manuscript concerns environmental and soil science and contains elements of computational methods, computer graphics and visualization.

Although the work is based on our master's thesis and Ph.D. dissertation, completed back in 1992-1993, we believe that its results have not lost their relevance.

The developed software (Turbo Pascal, total size 0.4 MB!) still runs on a modern computer inside DOSBox application. Finite element method execution, which used to take a significant amount of time on Intel, now takes seconds.

We provide the source codes in a public repository with details listed in the section "Code availability".

Thanks for your consideration.

Sincerely,

Igor Ratnere, Ph.D.
Lawrence Berkeley National Laboratory: E O Lawrence Berkeley National Laboratory
Berkeley, CA UNITED STATES
igorratn@yahoo.com

Highlights

Mathematical modeling of the impact of vehicles on water-saturated soil

Igor Ratnere, Ph.D.

- A method has been developed to assess the impact of a wheel on waterlogged forest soil.
- The form of the transverse loading diagram has a significant effect on the degree of the stress state of the soil.
- Tires with reduced internal air pressure have the least impact on the ground.
- An application has been developed to assess the degree of soil compaction and the intensity of rutting during the operation of a forest machine.

Mathematical modeling of the impact of vehicles on water-saturated soil

Igor Ratnere, Ph.D.[a]

[a] Igor Ratnere, Lawrence Berkeley National Laboratory, Berkeley, CA UNITED STATES, ORCID(s): 0000-0002-8098-3566

ARTICLE INFO

Keywords:

Soil mechanics

Water-saturated soil

Environmental impact of vehicle

Forest vehicle

The first boundary value problem

The finite element method

Level lines of a function

Authorship statement

The work was solely done by Igor Ratnere.

ABSTRACT

The presented mathematical model, together with its software implementation, makes it possible to assess the degree of influence of a vehicle on waterlogged forest soil, depending on the design parameters of the tire and the vertical loads on it.

The adequacy of the mathematical model is confirmed by the conducted experimental studies, as well as by numerous test results of forest machines.

The model is developed based on the theory of soil mechanics. The plane problem of compaction of water-saturated anisotropic (in the general case) soil is considered. It was shown that with an instantaneous application of a vertical load, the initial distribution of stress and water pressure in the soil are expressed through their values in a state of complete stabilization. Therefore, it is conventionally assumed that the magnitude of the load does not change before the onset of this state, causing linear (relative to the load) deformations of the soil.

Thus, first, a plane problem of different modulus of the theory of a linearly deformable medium is solved. This problem is described by a system of partial differential equations. The solution is found by the finite element method with respect to displacements. Then, the steady-state and initial values of the stresses are determined, as well as the values of the maximum deviation of the total stress vector.

In the case of an isotropic medium, the initial fluid head function (H_o) satisfies the Laplace equation: $\Delta H_o = 0$. The first boundary value problem is posed and solved. Analytical expressions are obtained for the initial values of heads and stresses. With their help, one can

select the optimal triangulation of the region for a given loading diagram and check the finite element solution.

The calculation results are presented as level lines of a function of two variables. The general view of the vertical stress function is in good agreement with the available experimental data.

It was found that the form of the transverse loading diagram has a significant effect on the degree of the stress state of the soil. At the same average contact pressures, the parabolic shape of the loading diagram, which is characteristic of tires with reduced internal air pressure, has the smallest effect on the soil.

The method can serve as the basis for predicting the degree of soil compaction and the intensity of rutting, as well as the environmental consequences of the operation of forest machines.

Introduction

The result of the harmful environmental impact of the skidder on the ground is soil compaction, destruction of sod cover, and rut formation. As shown by numerous observations in the USA, Canada and other countries, the use of a wheeled skidder in logging leads to soil compaction and, as a consequence, to a decrease in forest productivity. The operation of the machine causes compaction and destruction of the sod cover, which serves as the most important source of plant nutrition. There is a change in biogeochemical cycles, and seed germination worsens within the framework of natural reforestation.

Destruction of the upper sod layer, saturated with organic matter, occurs as a result of deepening the lugs and wheel slip. As the analysis of the impact of the wheel on the ground shows, the most important factors affecting the environmental consequences of movement are, on the one hand, the physical and mechanical properties of the soil, on the other hand, the ability of the wheel to realize the required traction force with minimal slipping and cause minimal soil compaction.

When solving the problem of reducing the impact of the wheel on the soil and assessing its state after the passage of the machine, the question naturally arises of identifying the factors affecting the deformation and compaction of the soil, and finding the mathematical relationships between them. The existing mathematical models of the interaction of the wheel with the ground are usually based on a one-dimensional stress distribution function over depth, which is obtained by processing the results of stamping tests (Ratnere, 1993). With this approach, it is impossible to assess the plane and spatial phenomena, including the distribution of compaction zones under the wheel and edge effects that cause lateral uplift of the soil. In addition, the whole principle of constructing the model is based on the mechanical transfer of the results of stamp tests to the wheel rolling process, it does not reflect the dynamics of the phenomenon, and the complication of the model by the introduction of correction factors for the geometric parameters of the contact patch and the time of application of the load does not contribute to an increase in the accuracy of the solution, since their influence on the final result is nullified by averaging the load over the contact patch and the accuracy of obtaining soil characteristics. Therefore, it is necessary to look for new methods of constructing a mathematical model.

The basis for the construction of a mathematical model was a well-developed theory of soil mechanics. Its methods have been successfully applied in practice for a long time. There are proven methods for obtaining the required characteristics of soils and an extensive data on them.

The mathematical model, together with its software implementation, allows:

1) To judge the influence of the design features of the wheels and the nature of the vertical load on the distribution of stresses in the soil.

2) Take into account the anisotropy of soil properties.

3) Simulate movement on ice and swamp.

4) Assess the ability and environmental impact of vehicle on soft ground.

5) Predict the degree of soil compaction and the intensity of rutting during the operation of the forest machine.

1. Basic concepts of the physical and mechanical properties of soil

By their nature, soils are divided into two main classes: sands are products of mechanical destruction of basic rocks, and clays are products of chemical destruction of basic rocks. Sands and clays differ greatly in their physical and mechanical properties.

In nature, soils of mixed origin are usually found. They exhibit intermediate properties of sand and clay and are called, respectively, sandy loam, loam, etc.

All qualitative differences in soil properties are determined by the size and shape of the particles forming them. Of great importance in the manifestation of these properties is the water in the gaps between the particles. The gas in the soil (air, methane, water vapor) also strongly affects the properties of the soil.

Sands consist of particles having the shape of grains with a diameter of 0.5 - 2 mm (coarse sand) to 0.1 - 0.05 mm (fine sand) (Florin, 1954). Clay particles are in the form of plates with a thickness of not more than 1 micron.

Let us introduce the notation.

V - some volume of soil;

V_p - pore volume;

V_s - volume of solid particles;

$V = V_p + V_s$;

$n = \frac{V_p}{V}$ - soil porosity;

$m = \frac{V_s}{V}$ - the volume of solid particles per unit volume of soil;

$n + m = 1$;

$\varepsilon = \frac{V_p}{V_s} = \frac{n}{m}$ - coefficient of porosity.

Compressibility of soils.

Due to the low permeability of solid soil particles, compression deformation occurs mainly due to a change in porosity. The relationship between the coefficient of porosity ε and compressive stresses σ is obtained using uniaxial compression devices (Figure 1.1).

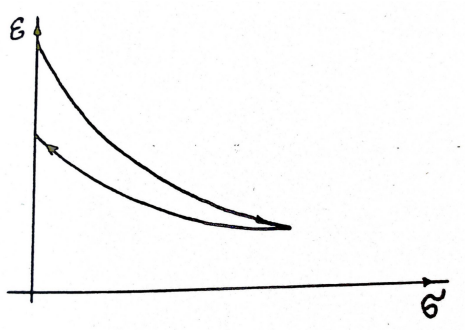

Figure 1.1: Compression curve.

On small intervals of stresses change, it is approximated by a straight line

$$\varepsilon = -a\sigma + A \quad . \tag{1}$$

With a large number of loading and unloading, the soil becomes practically elastic.

Weakly compacted clays	0.10 - 0.01
Compacted clays	0.005 - 0.001

Compaction factors a, cm^2/kg (Florin, 1954).

Sands	0.54 - 0.82
Compacted clays	0.67 - 1.2
Silt	1.00 - 3.00
Loams and clays	0.67 -1.00

Porosity coefficients ε *(Florin, 1954).*

Filtration properties of soils.

The filtration rate is defined in soil mechanics as the flow rate of water through a unit of the geometrical area of the soil section. Darcy's law establishes a relationship between the filtration rate u and the fluid pressure gradient H :

$$u = -k \frac{\partial H}{\partial s} \quad ,$$

where k is the filtration coefficient (cm / s).

H is determined in hydraulics by the formula:

$$H = \frac{P}{\gamma} + z \quad , \text{(cm)}$$

where P is the pressure in the liquid (kg/cm^2),

γ - specific gravity of the liquid (kg/cm^3),

z - the height of this point above the zero mark (cm).

The actual speed of water relative to immobile soil grains is determined by the formula:

$$u_a = \frac{u}{n} \quad ,$$

where is n the porosity of the soil (see above).

In the case of movement of soil grains towards the liquid at a speed, v_a Darcy's law is written in the form:

$$u_a - v_a = -\frac{k}{n} \frac{\partial H}{\partial s} \Rightarrow u - \varepsilon v = -k \frac{\partial H}{\partial s} \quad . \qquad (2)$$

Sands	$10^{-2}-10^{-3}$
Clays	$10^{-6}-10^{-8}$

Filtration coefficient k , cm / s (Florin, 1954).

Understanding stresses in soil.

Consider the case of deformation propagation in one plane. Let's select an elementary parallelepiped and call the ratio of the force acting on an elementary area to its area stress. Then, on the sections of the parallelepiped, inclined at different angles, we will get different values of stresses. The stress vector coincides in direction with the force vector and it can be decomposed into normal and tangential components: σ_n and τ (Figure 1.2).

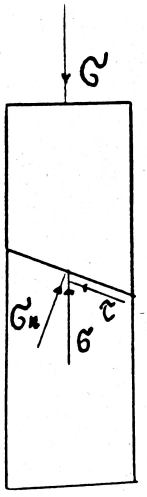

Figure 1.2 Plane stresses.

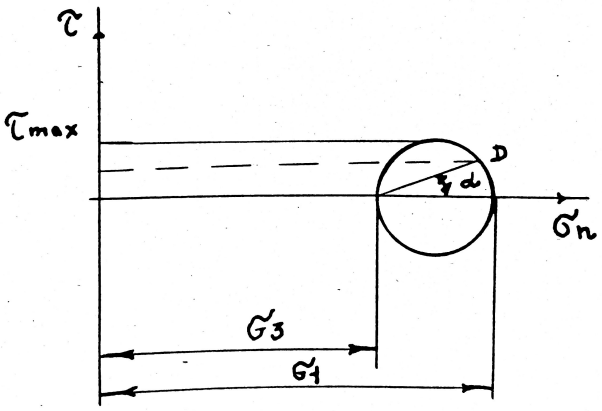

Figure 1.3 Mohr's circle.

Let us introduce a rectangular coordinate system XoZ and denote the stresses acting along the oX and oZ axes, respectively, σ_x and σ_z .

Let only normal stress act in some section, and there is no tangential stress. This normal stress is called the principal one. The largest and the smallest normal stresses acting in a given section are the principal ones. They are denoted by σ_1 and σ_3 respectively.

It is convenient to determine the stress distribution in the sections of an elementary parallelepiped using Mohr's circles (Figure 1.3).

It can be seen from the figure that in the section drawn at an angle α , the values of the normal and tangential stresses are determined by the coordinates of the point D on the circle. The maximum shear stress in absolute value is achieved at $\alpha=\pm\pi/4$.

The concept of soil strength.

In soil mechanics, the main indicators of strength are considered to be the shear resistance of the soil. The maximum shear stress is determined from the equation:

$$\tau = c + \sigma_n \tan\varphi \quad , \tag{3}$$

where c is called adhesion, and φ is the angle of internal friction. For sands $c=0$, therefore $\tau=\sigma_n \tan\varphi$. The φ angle for sands is a constant value , while for clays the cohesion and the angle of internal friction depend on the density and moisture. After preliminary compaction of the soil, an increase in adhesion and a decrease in the angle of internal friction are observed, this is due to an irreversible decrease in the coefficient of porosity ε , as a result of which the molecular forces of interaction between particles increase (Pokrovsky, 1941).

From equation (3), you can determine the straight lines, which are called the lines of destruction. For a given value σ_1 , construct a Mohr circle so that it touches these lines (Figure 1.4).

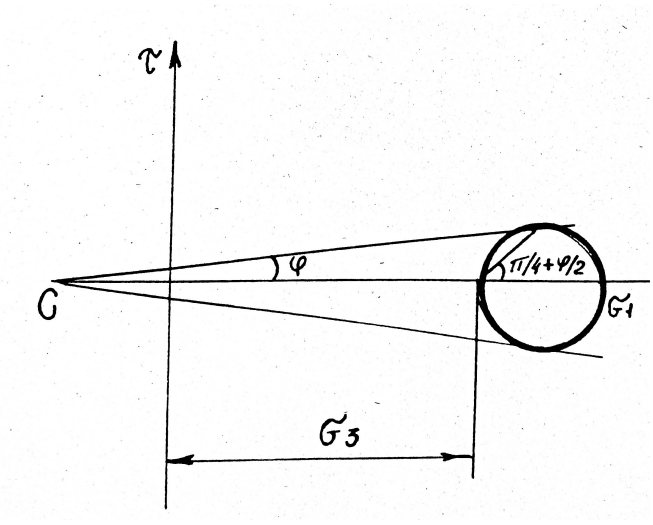

Figure 1.4 Plastic limit equilibrium.

201

202 The slope of the fracture planes can now be determined. It makes an angle $\pi/4+\varphi/2$ to the
203 line of action of the lowest principal stress. At this moment, the principal stresses satisfy the
204 equation

$$\sigma_1 = 2c\sqrt{\lambda_\varphi} + \sigma_3\lambda_\varphi \quad , \tag{4}$$

205

206 where $\lambda_\varphi = \tan^2(\pi/4+\varphi/2)$, and the soil massif is in a state of so-called plastic limiting
207 equilibrium (Terzagi, 1961). The effect of the hydrostatic pressure of water in the pores of the
208 soil should also be taken into account, therefore, the so-called effective stress, which is perceived
209 by the skeleton of the soil, should be substituted in formulas (3) and (4), and their values are less
210 than the actual stresses by the value of the pore pressure of water. The sine of the largest
211 deviation of the total stress vector can be represented as:

212 $$\sin\theta_{max} = \frac{\sqrt{(\sigma_x-\sigma_z)^2+4\tau_{xz}^2}}{\sigma_z+\sigma_x+2c/\tan\varphi} \quad .$$

213 Deformation modulus and Poisson's ratio.

214 When compressing a soil sample in a compression device, transverse deformations of the soil are

impossible. In this case, the lateral pressure coefficient ζ is determined by the formula:

$\zeta=\frac{\sigma_x}{\sigma_z}$. In soil mechanics, it is assumed that porosity depends only on the sum of the principal stresses, and not on their ratios. This assumption is based on the approximation of the real stress-strain curve by a straight line with sufficient accuracy for practical calculations. Because of this, we write formula (1) for the case of a biaxial stress state (plane problem):

$$\varepsilon=-a\frac{\theta}{1+\zeta}+A \quad , \tag{5}$$

here $\theta=\sigma_x+\sigma_z$ is the sum of the principal stresses.

The deformation modulus $E(\varepsilon)$ is determined in soil mechanics from the expression:

$$de_x=\frac{d\sigma_x-\nu d\sigma_z}{E(\varepsilon)} \quad ,$$

where σ_x and σ_z is the increment in stresses, that caused de_x - the strain increment along the oX axis.

Poisson's ratio ν is defined through the lateral pressure coefficient ζ : $\nu=\frac{\zeta}{1+\zeta}$.

If we take the dependence $\varepsilon=\varepsilon(\theta)$ as linear, for example, in the form (5), we obtain

$$E=\frac{\beta(1+\varepsilon)}{a} \quad ,$$

where $\beta=\frac{(1-\zeta)(1+2\zeta)}{(1+\zeta)}$.

Sands	0.40-0.42
Clays	0.70-0.75

Lateral pressure coefficient (Florin, 1954).

The above expressions for the deformation moduli make it possible, in the case of a nonlinear relationship between stresses and strains, to determine the modulus value for any given stress

state. However, in many cases it is more convenient to use the so-called average deformation modulus

$E_{avg}=\frac{\beta(1+\varepsilon_1)}{a}$, where ε_1 is the initial porosity coefficient.

It was shown (Gersevanov, 1948) the constancy of E_{avg} for plastic soils in a small range of load variation, which indicates a linear relationship between stresses in the skeleton and its deformations, and this shows that the formulas of the theory of elasticity are applicable to the calculations of stresses and deformations in the soil skeleton.

In conclusion, let us consider the case of applying a vertical load along the rectilinear boundary of a linearly deformed medium. In this case (Timoshenko and Goodier, 1970):

$$\sigma_x=\frac{1}{2}\theta+\frac{1}{2}z\frac{\partial\theta}{\partial z} \quad ,$$

$$\sigma_z=\frac{1}{2}\theta-\frac{1}{2}z\frac{\partial\theta}{\partial z} \quad , \qquad (6)$$

$$\tau_{xz}=-\frac{1}{2}z\frac{\partial\theta}{\partial x} \quad .$$

The stress components are determined by the formulas:

$$\sigma_x=\lambda e+\nu\varepsilon_x \quad ,$$

$$\sigma_z=\lambda e+\nu\varepsilon_z \quad ,$$

where $\varepsilon_x=\frac{\partial u_1}{\partial x}$, $\varepsilon_z=\frac{\partial u_3}{\partial z}$, $\lambda=\frac{\nu E}{(1+\nu)(1-2\nu)}$, $e=\varepsilon_x+\varepsilon_z$,

u_1 и u_3 - displacement components.

$$\tau_{xz}=\nu\gamma_{xz} \quad ,$$

where $\gamma_{xz} = \frac{\partial u_1}{\partial z} + \frac{\partial u_3}{\partial z}$.

For a general model of a linearly deformable medium, the stresses in the soil skeleton must satisfy the equations (Timoshenko and Goodier, 1970):

$$\frac{\partial \sigma_x}{\partial x} + \frac{\partial \tau_{xz}}{\partial z} + X = 0 \quad , \tag{7}$$

$$\frac{\partial \tau_{xz}}{\partial x} + \frac{\partial \sigma_z}{\partial z} + Z = 0 \quad , \tag{8}$$

where X и Z - components of volumetric forces,

along with the equation

$$\Delta(\sigma_x + \sigma_z) = -\frac{1}{1-\nu}\left(\frac{\partial X}{\partial x} + \frac{\partial Z}{\partial z}\right) \quad , \tag{9}$$

where ν - коэффициент Пуассона ;

Δ - оператор Лапласа.

2. Mathematical formulation of the compaction problem

2.1. The Simplest One-Dimensional Compaction Problem

Key assumptions:

a) We consider models of a two-component soil consisting of solid particles and water filling its pores. This model is called soil mass. “The question may arise: in what cases, in practice, are we dealing with a soil mass? ... As for the ground lying above the groundwater level, in the vast

majority of cases it is a soil mass, that is, one in which all voids are filled with water due to the capillary rise of water in the fine pores of the soil. In clays, the length of the capillary rise of water can reach a height of over 300 m above the groundwater level.

In order to judge whether we have a soil mass above the groundwater level, we can be guided by the following signs: in all cases when the soil is in a fluid, plastic and semi-solid state, we are dealing with a soil mass. Only when the soil passes from a semi-solid state to a solid state does air penetrate into the pores of the soil and partially fill the voids of the soil skeleton. The transition from solid to solid is characterized by a sharp change in the color of the soil. … To determine the condition of the soil, i.e. whether it is fluid, plastic or semi-solid, there are fully developed laboratory methods ... ”(Gersevanov, 1948, p. 145).

b) The change in porosity occurs only due to the dense packing of soil particles;

c) The filtration coefficient does not depend on the stress state.

Basic equations.

1. Equations of continuity for solid and liquid soil components.

$$\frac{\partial u_z}{\partial z}+\frac{\partial n}{\partial t}=0 \quad , \tag{1}$$

$$\frac{\partial v_z}{\partial z}+\frac{\partial m}{\partial t}=0 \quad , \tag{2}$$

here, as before, v_z u_z and are the flow rates of the solid and liquid components along the oZ axis. Adding equations (1), (2) and taking into account equality $n+m=1$, we obtain

$$\frac{\partial u_z}{\partial z}+\frac{\partial v_z}{\partial z}=0 \quad . \tag{3}$$

283

284 2. Darcy's dependency.

$$u_z - \varepsilon v_z = -k \frac{\partial H}{\partial z} \quad . \tag{4}$$

285

286 3. Equilibrium equation.

287 Let σ - stress in the soil skeleton; p - pressure in water; σ^* and p^* - the corresponding

288 values in a state of complete stabilization.

$$\sigma + p = \sigma^* + p^* \quad . \tag{5}$$

289 That is the sum of stress and pressure is a constant.

290 Differentiate (4) by z :

291 $$\frac{\partial u_z}{\partial z} - \frac{\partial \varepsilon}{\partial z} v_z - \varepsilon \frac{\partial v_z}{\partial z} = -\frac{\partial}{\partial z}\left(k \frac{\partial H}{\partial z}\right) \quad ,$$

292 considering (3):

293 $$v_z \frac{\partial \varepsilon}{\partial z} + (1+\varepsilon) \frac{\partial v_z}{\partial z} = \frac{\partial}{\partial z}\left(k \frac{\partial H}{\partial z}\right) \quad .$$

294 Further, taking into account (2) and the relationship between ε and m from Section 1, we

295 obtain:

296 $$\frac{\partial v_z}{\partial z} = -\frac{\partial m}{\partial t} = -\frac{\partial}{\partial t}\left(\frac{1}{1+\varepsilon}\right) = \frac{1}{(1+\varepsilon)^2} \frac{\partial \varepsilon}{\partial t} \quad ;$$

297

298 $$v_z \frac{\partial \varepsilon}{\partial z} + (1+\varepsilon) \frac{\partial v_z}{\partial z} = \frac{\partial}{\partial z}\left(k \frac{\partial H}{\partial z}\right) \quad .$$

299 Further, as shown in Florin (1961),

300 $$v_z \frac{\partial \varepsilon}{\partial z} = o\left(\frac{\partial \varepsilon}{\partial t}\right)$$

301 and the error from replacement $[1+\varepsilon(t,z)]$ by $[1+\varepsilon(t,z)]$ (ε is the average porosity in

302 the considered compaction range) is less than the error of the laboratory determination of the

303 filtration coefficient k .

304 In view of the above

305 $$\frac{\partial \varepsilon}{\partial z} = (1+\varepsilon)\frac{\partial}{\partial z}\left(k\frac{\partial H}{\partial z}\right) ,$$

306 $$\frac{\partial \varepsilon}{\partial t} = \frac{d\varepsilon}{d\sigma}\frac{\partial \sigma}{\partial t} = -a\left(-\frac{\partial p}{\partial t}\right) = a\gamma\frac{\partial H}{\partial t} .$$

307 Here we used equation (1) from Section 1 and equilibrium equation (5). We will finally write

308 down

$$\frac{\partial H}{\partial t} = \frac{(1+\varepsilon)}{a\gamma}\frac{\partial}{\partial z}\left(k\frac{\partial H}{\partial z}\right) . \qquad (6)$$

309

310 The resulting equation is equivalent in form to the equation of heat conduction and diffusion.

311 Next, the initial and boundary conditions are assigned:

312 $t=0,\ H=H(Z)$;

313 $t>0,\ z=0:\ H=\lambda(t),\ z=z^*:\ H=\mu(t)$.

314 Example. Let the distributed load $q:\ H_o=q/\gamma$ be instantaneously applied at the initial

315 moment $t=0$. If the layers $z=0$ and $z=z^*$ are also permeable, then when $t>0$:

316 $z=0,\ H=0;\ z=z^*,\ H=0$,

317 For waterproof layers $\frac{\partial H}{\partial z}=0$.

318 The solution of equation (6) together with the given initial and boundary conditions is found by

known methods, for example, by the method of separation of variables (by the Fourier method).

The stress distribution $\sigma(z,t)$ is determined from equation (5):

$$\sigma + p = const = q \quad ,$$

$$\sigma = q - p = q - \gamma H \quad .$$

The amount of compaction can be found by the formula:

$$s(t,h) = \int_o^h e_z(t,z)\,dz \quad ,$$

where e_z is the compaction of the layer with the coordinate z, according to the results of

Section 1, $e_z = \frac{a}{1+\varepsilon}\sigma$;

h - active compaction depth, can be determined in the following way:

make up a sequence $(h_k), k = 0,1,2...$ and determine h_l from the condition:

$$\frac{|s(t,h_{l-1}) - s(t,h_l)|}{s(t,h_l)} \le \delta \quad .$$

Where δ is the specified accuracy. Thus, the problem of compaction in the one-dimensional case can be considered solved.

2.2. Plane and spatial problems of compaction

The assumptions are the same as in the previous paragraph. First, consider the planar compaction problem (XoZ plane).

Basic equations.

1. Equations of continuity

$$\frac{\partial u_x}{\partial x} + \frac{\partial u_z}{\partial z} + \frac{\partial n}{\partial t} = 0 \qquad (1)$$

$$\frac{\partial v_x}{\partial x}+\frac{\partial v_z}{\partial z}+\frac{\partial m}{\partial t}=0 \quad . \tag{2}$$

337

338 Add equations (1), (2)

$$\frac{\partial (u_x+v_x)}{\partial x}+\frac{\partial (u_z+v_z)}{\partial z}=0 \quad . \tag{3}$$

339

340 2. Darcy's dependence

$$u_x-\varepsilon v_x=-k\frac{\partial H}{\partial x} \tag{4}$$

$$u_z-\varepsilon v_z=-k\frac{\partial H}{\partial z} \quad . \tag{5}$$

341 3. Equilibrium equations

$$\sigma_x+p=\sigma_x^*+p^* \tag{6}$$

$$\sigma_z+p=\sigma_z^*+p^* \tag{7}$$

$$\tau_{xz}=\tau_{xz}^* \quad . \tag{8}$$

342 Here τ_{xz} are the shear stresses. It is assumed that the tangential load is instantly perceived by

343 the skeleton and is not transmitted to the water.

344 Differentiate (4) by x , (5) by z and add up:

345 $$\frac{\partial u_x}{\partial x}+\frac{\partial u_z}{\partial z}-\varepsilon(\frac{\partial v_x}{\partial x}+\frac{\partial v_z}{\partial z})=-[\frac{\partial}{\partial x}(k\frac{\partial H}{\partial x})+\frac{\partial}{\partial z}(k\frac{\partial H}{\partial z})] \quad .$$

346 Comment. Discarded terms $\frac{\partial \varepsilon}{\partial z}v_z$ and $\frac{\partial \varepsilon}{\partial x}v_x$.

347 Taking into account (3), we obtain

348 $$(1+\varepsilon)(\frac{\partial v_x}{\partial x}+\frac{\partial v_z}{\partial z})=\frac{\partial}{\partial x}(k\frac{\partial H}{\partial x})+\frac{\partial}{\partial z}(k\frac{\partial H}{\partial z}) \quad ,$$

349 where the value $1+\varepsilon$ is a constant (see section 2.1).

350 Further, from (2) we have

351 $$\frac{\partial v_x}{\partial x}+\frac{\partial v_z}{\partial z}=-\frac{\partial m}{\partial t}=\frac{1}{(1+\varepsilon)^2}\frac{\partial \varepsilon}{\partial t} \quad ,$$

352 taking this into account, we get

$$\frac{\partial \varepsilon}{\partial t}=(1+\varepsilon)[\frac{\partial}{\partial x}(k\frac{\partial H}{\partial x})+\frac{\partial}{\partial z}(k\frac{\partial H}{\partial z})] \quad . \tag{9}$$

353

354 Next, we use equation (5) from Section 1.1. We have

355 $$\frac{\partial \varepsilon}{\partial t}=\frac{d\varepsilon}{d\sigma}\frac{\partial \sigma}{\partial t}=-\frac{a}{1+\xi}\frac{\partial \theta}{\partial t} \quad .$$

356 From equations (6) and (7) we obtain

357 $$\theta=\sigma_x+\sigma_z=\theta^*=\sigma_x^*+\sigma_z^*-2(p-p^*) \quad ,$$

358 thus it turns out

359 $$\frac{\partial \theta}{\partial t}=-2\frac{\partial p}{\partial t}=-2\gamma\frac{\partial H}{\partial t} \quad .$$

360 Let us finally write equation (9) in the form:

$$\frac{\partial H}{\partial t}=\frac{(1+\varepsilon)(1+\xi)}{2\gamma a}[\frac{\partial}{\partial x}(k\frac{\partial H}{\partial x})+\frac{\partial}{\partial z}(k\frac{\partial H}{\partial z})] \quad . \tag{10}$$

361

362 Reasoning quite similarly in the case of a triaxial stress state, we arrive at the equation:

$$\frac{\partial H}{\partial t}=\frac{(1+\varepsilon)(1+2\xi)}{3\gamma a}[\frac{\partial}{\partial x}(k\frac{\partial H}{\partial x})+\frac{\partial}{\partial y}(k\frac{\partial H}{\partial y})+\frac{\partial}{\partial z}(k\frac{\partial H}{\partial z})] \quad . \tag{11}$$

363

364 Let us assume that the filtration coefficient k does not change during the compaction process.

365 Then we have:

$$\frac{\partial H}{\partial t}=K\Delta H \quad . \tag{12}$$

366

367 Where Δ is the Laplace operator,

368 $K=\frac{(1+\varepsilon)(1+\xi)}{2\gamma a}k$ - for a plane problem

369 $K=\frac{(1+\varepsilon)(1+2\xi)}{3\gamma a}k$ - for a spatial problem.

370 Initial conditions.

371 Note that the initial heads distribution function H_o satisfies the Laplace equation

$$\Delta H_o=0 \quad . \tag{13}$$

372

373 This equation is a consequence of the fact that at the initial moment of load application

374 $$\frac{\partial v_x}{\partial x}=\frac{\partial v_y}{\partial y}=\frac{\partial v_z}{\partial z}=0 \quad .$$

375 We find the initial pressure distribution from (6) and (7):

376 in the case of the plane problem

$$P_o=\frac{1}{2}\theta_o^*+P_o^* \quad , \tag{14}$$

377 for a spatial task

$$P_o=\frac{1}{3}\theta_o^*+P_o^* \quad . \tag{15}$$

378 Here, as before, θ_o^* denotes the sum of normal stresses in a stabilized state, P_o^* is the final

379 pressure distribution. We accept further $P_o^*=0$.

380 Thus, to determine the initial distribution of the pressure, it is necessary to solve problems (7),

381 (8) and (9) of the theory of elasticity (Section 1).

382 The initial stress distribution is determined from (6), (7), (14), (15)

383 for a planar problem

384 $$\sigma_{xo}=\frac{1}{2}(\sigma_x^*-\sigma_z^*) \quad ,$$

$$\sigma_{zo}=\frac{1}{2}(\sigma_z^*-\sigma_x^*) \quad ,$$

$$\tau_{xzo}=\tau_{xz}^* \quad .$$

For a spatial problem

$$\sigma_{xo}=\sigma_x^*-\frac{1}{3}\theta_o^* \quad ,$$

$$\sigma_{yo}=\sigma_y^*-\frac{1}{3}\theta_o^* \quad ,$$

$$\sigma_{zo}=\sigma_z^*-\frac{1}{3}\theta_o^* \quad ,$$

$$\tau_{xzo}=\tau_{xz}^*, \quad \tau_{xyo}=\tau_{xy}^*, \quad \tau_{yzo}=\tau_{yz}^* \quad .$$

Border conditions .

On the permeable sections of the boundary surface, the values of the pressure function are equal to zero: $H=0,\ x\in\Gamma$. In watertight areas, the pressure gradient value is zero:

$$\frac{\partial H}{\partial n}=0,\ x\in\Gamma \quad .$$

In addition, in the case of compaction of heterogeneous soil, the conjugation conditions must be met at the border of adjacent media:

$$H_1(x,t)|_S=H_2(x,t)|_S \quad ;$$

$$k_1(\frac{\partial H_1}{\partial n})=k_2(\frac{\partial H_2}{\partial n}) \quad .$$

Example. The plane problem of compaction of isotropic soil with an arbitrary vertical load. We find the initial stress distribution from equation (6) in Section 1 and from equations (6), (7), (8):

$$\sigma_{xo}=\frac{1}{2}(\sigma_x^*-\sigma_z^*)=\frac{1}{2}z\frac{\partial\theta^*}{\partial z}=z\frac{\partial P_o}{\partial z}$$
$$\sigma_{zo}=\frac{1}{2}(\sigma_z^*-\sigma_x^*)=-z\frac{\partial P_o}{\partial z} \quad . \tag{16}$$
$$\tau_{xzo}=\tau_{xz}^*=\frac{1}{2}z\frac{\partial\theta^*}{\partial x}=-z\frac{\partial P_o}{\partial z}$$

402

403 To determine P_o , it is necessary to solve the following problem:

404 $$\Delta P_o=0 \quad ,$$

405 $z=0,\ x\in D \quad P_0=q(x)$ - given load,

$$\begin{array}{c} x\notin D \quad P_o=0; \\ x\to\pm\infty, \quad z\to\pm\infty, \quad P_o=0 \end{array} \quad . \tag{17}$$

406

407 Consider a more general first boundary value problem:

$$\begin{array}{c} Lu=-f(M), \quad (M\in D) \\ u|_S=\varphi(M) \end{array} \quad . \tag{18}$$

408 In the original problem

409 $$u\equiv H, \quad Lu=\Delta u=\frac{\partial^2 u}{\partial x^2}+\frac{\partial^2 u}{\partial z^2} \quad ;$$

410 $$f(M)=f(x,z)=0, (M\in D) \quad ;$$

411 $$\varphi(M)=\varphi(x,z) \quad \equiv \quad \begin{cases} 0, z=0, x\notin[-a,a] \\ q(x), z=0, x\in[-a,a] \\ 0, z\to+\infty, x\to\pm\infty \end{cases} ,$$

412 where $q(x)=\gamma\varrho(x)$ is the diagram of the load distribution, 2a is the contact width (Figure

413 2.1).

414

415

416

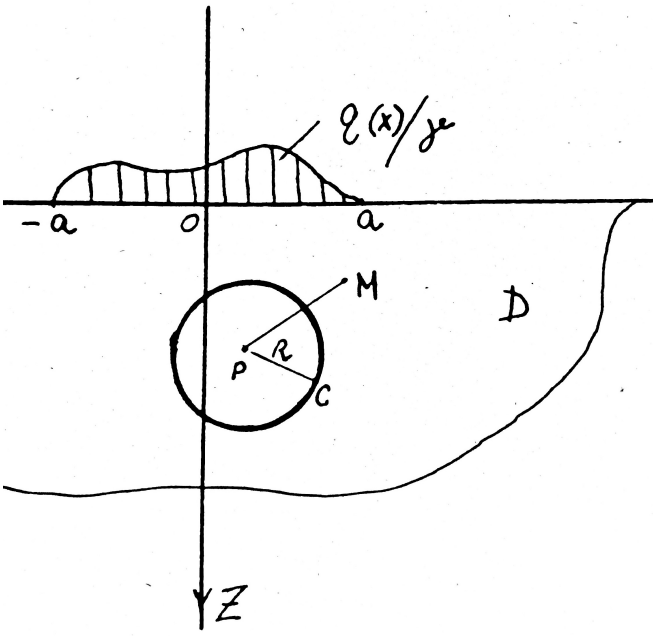

Figure 2.1 On the definition of the Green's function.

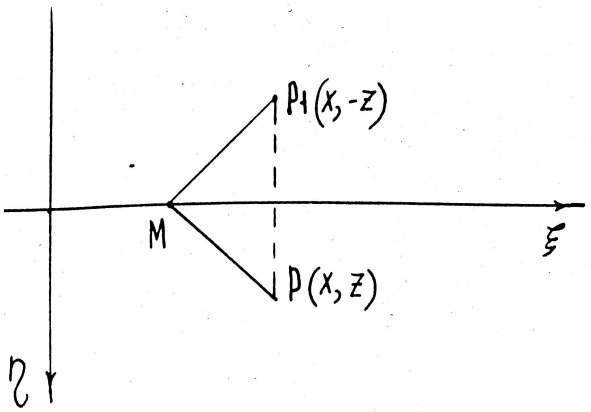

Figure 2.2 Reflection method.

417

418 To solve problem (18), the method of Green's functions is used, the solution has the form

419 (Nikiforov, 1983):

420 $$u(P)=-\int_S \varphi \frac{\partial G}{\partial n} dS_M$$

421 where $G=G(M,P)$ is the solution to an equation of a special form:

$$\begin{cases} \Delta G=-\delta(M,P) \ (M\in D) \\ G|_S=0 \end{cases} . \qquad (19)$$

422

423 Here $\delta(M,P)$ is the Dirac δ - function. Solution (19) is presented in the form:

424 $$G(M,P)=\psi(\Gamma_{MP})+V(M,P) \ ,$$

425 where V is harmonious at D (i.e. $\Delta V=0, M\in D$), and $\psi(\Gamma_{MP})$ has a singularity at the

point P and at $\Gamma_{MP}=0$

$$\Delta\psi=-\delta(M,P) \quad . \tag{20}$$

We integrate (20)

$$\int_{S_P^R}\Delta\psi\,ds=-1 \quad (\ \delta\ \text{- function property}).$$

Using Green's formula, we pass to the integral over a circle centered at the point P of radius R (see Figure 2.1):

$$\oint_C\frac{\partial\psi}{\partial n}ds=\oint_C\frac{d\psi}{dr}ds=\frac{d\psi}{dr}|_R\cdot 2\pi R=-1$$

$$d\psi(R)=-\frac{1}{2\pi}\frac{dR}{R}\Rightarrow\psi(R)=-\frac{1}{2\pi}\ln\frac{1}{R} \quad .$$

$$\Rightarrow G(M,P)=\frac{1}{2\pi}\ln(\frac{1}{\Gamma_{MP}})+V(M,P)$$

For our case $V(M,P)$ is determined by the method of reflections (Figure 2.2).

Due to the fact that on the boundary of the half-plane $G(M,P)=0$, it follows that

$V(M,P)=-\frac{1}{2\pi}\ln(\frac{1}{\Gamma_{MP_1}})$ is a harmonic function $\forall M\in D$.

$$\Rightarrow G(M,P)=\frac{1}{2\pi}\ln(\frac{1}{\Gamma_{MP}})-\frac{1}{2\pi}\ln(\frac{1}{\Gamma_{MP_1}}) \quad ,$$

or in coordinates $x,z,\xi,\eta:(M(\xi,\eta),P(x,z))$:

$$G(M,P)=\frac{1}{2\pi}\ln(\frac{1}{\sqrt{(x-\xi)^2+(z-\eta)^2}})-\frac{1}{2\pi}\ln(\frac{1}{\sqrt{(x-\xi)^2+(z+\eta)^2}})$$

$$\Rightarrow u(P)=-\int_a^{-a}\varrho(\xi)\frac{\partial G}{\partial\eta}|_{\eta=0}d\eta \quad ,\ \text{and it remains to find}$$

$$\frac{\partial G}{\partial\eta}|_{\eta=0}=\frac{1}{2\pi}\ln(\frac{2z}{(x-\xi)^2+z^2}) \quad .$$

Thus, the solution (18) is:

$$H_o(x,z)=\frac{1}{\pi}\int_a^{-a}\varrho(\xi)\frac{z}{(x-\xi)^2+z^2}d\xi \quad .$$

For the original problem, this is equivalent to the following expression:

$$H_o(x,z)=\frac{1}{\pi}\int_a^{-a}\varrho(\xi)\frac{z}{(x-\xi)^2+z^2}d\xi \quad .$$

So found in the initial pressure distribution:

$$P_o(x,z)=\frac{\gamma}{\pi}\int_a^{-a}\varrho(\xi)\frac{z}{(x-\xi)^2+z^2}d\xi \quad ,$$

where $\varrho(\xi)=\frac{q(\xi)}{\gamma}$, that is, you can rewrite

$$P_o(x,z)=\frac{1}{\pi}\int_a^{-a}q(\xi)\frac{z}{(x-\xi)^2+z^2}d\xi \quad . \qquad (21)$$

We find the initial stress distribution by the formulas (16):

$$\sigma_{xo}=z\frac{\partial P_o}{\partial z}=\frac{z}{\pi}\int_{-a}^{a}q(\xi)\frac{(x-\xi)^2-z^2}{[(x-\xi)^2+z^2]^2}d\xi$$

$$\sigma_{zo}=-\sigma_{xo} \qquad . \qquad (22)$$

$$\tau_{xzo}=-z\frac{\partial P_o}{\partial z}=\frac{1}{\pi}\int_{-a}^{a}q(\xi)\frac{2z(x-z)}{[(x-\xi)^2+z^2]^2}d\xi$$

The distribution of initial stresses and pressures for an arbitrary vertical load is shown in Figures 2.3 and 2.4.

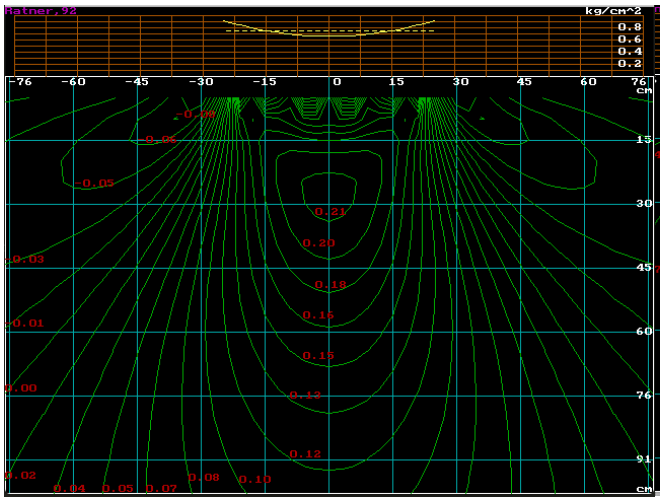

Figure 2.3 Distribution of initial stresses $\sigma_{zo}, kg/cm^2$ *in a homogeneous environment.*

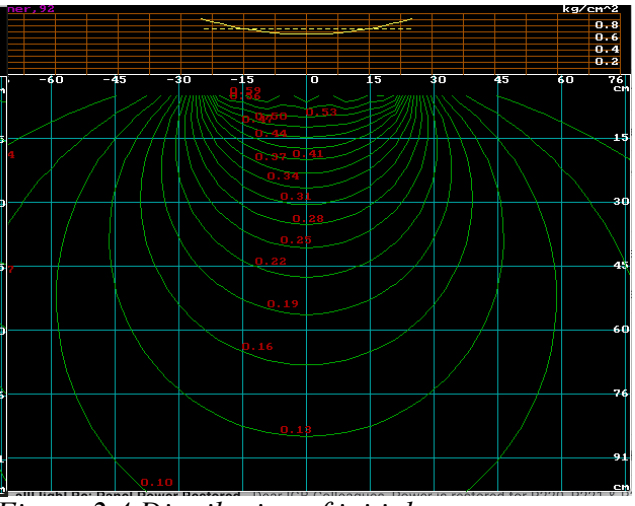

Figure 2.4 Distribution of initial pressures $(P_o, kg/cm^2)$ *in a homogeneous environment.*

3. Finite-element solution of a multimodular problem of the theory of elasticity

The initial conditions of problem (12) in Section 2 are expressed in terms of the steady-state stress distribution, the definition of which is devoted to this section.

Earlier it was indicated (Section 1) that the formulas of the theory of elasticity are formally applicable to the calculation of stresses and strains in the soil skeleton, although in essence it means the presence of not elastic, but a linear relationship between stresses and deformations.

Select a rectangular area on the half-plane and triangulate it (Figure 3.1).

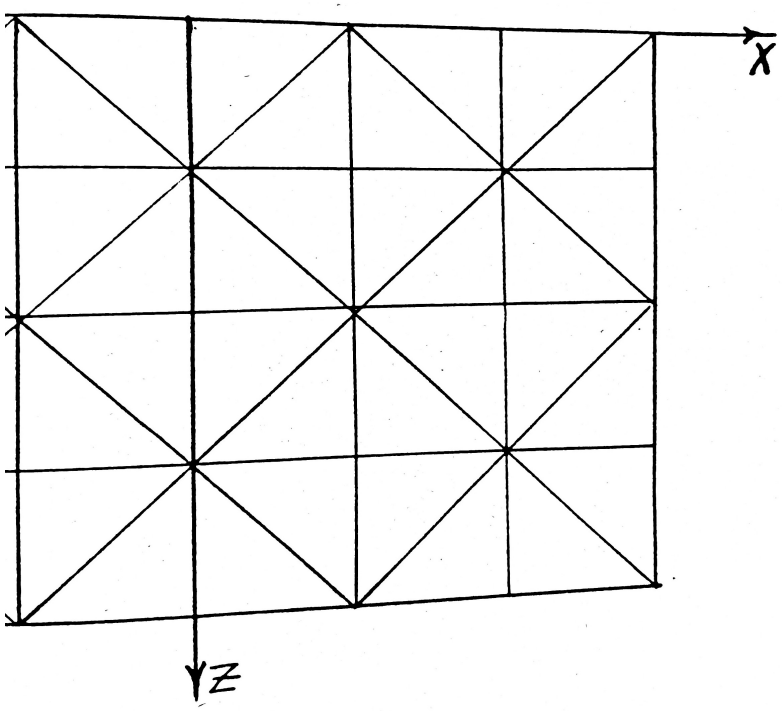

Figure 3.1 Area triangulation.

464 Consider the four types of triangles used in the partition. The nodes are numbered clockwise

465 (Figure 3.2).

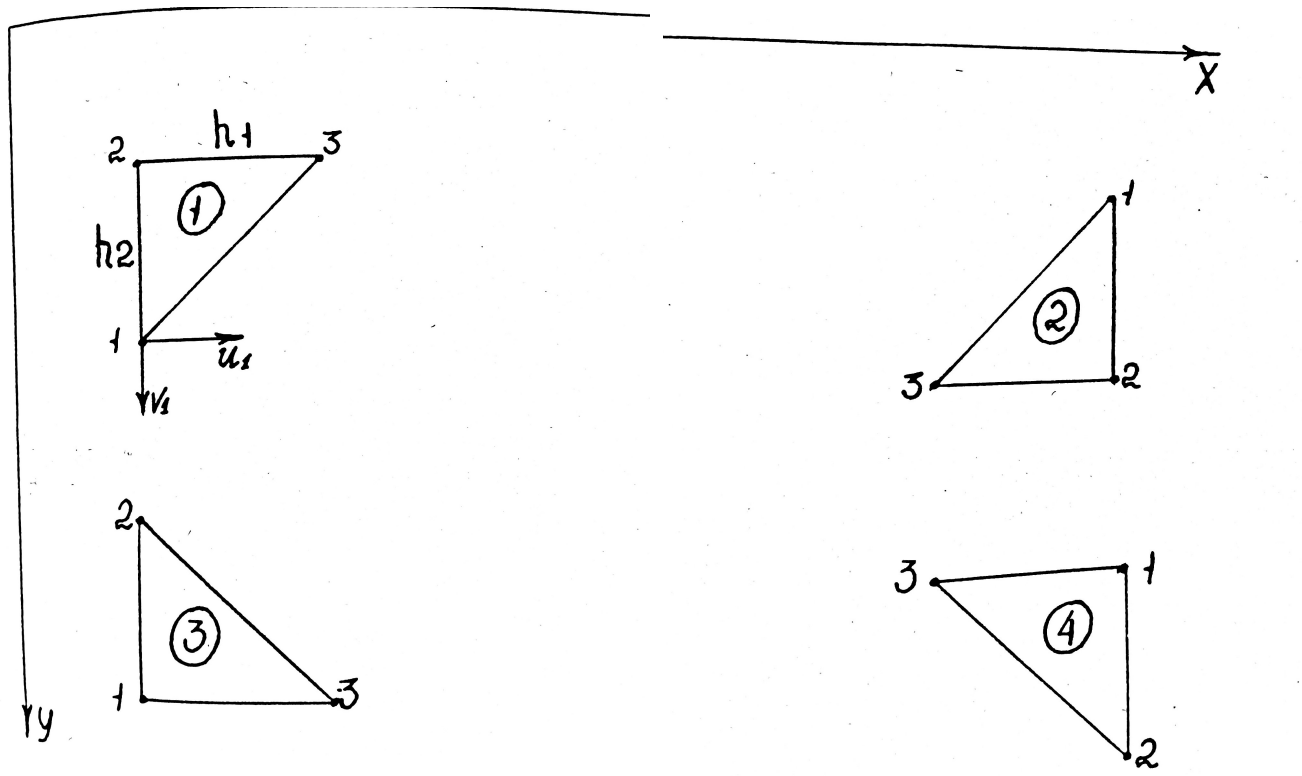

Figure 3.2 Types of triangulation elements.

We denote the movement of the i-th node of a separate element through u_i and v_i . The displacements of the nodes belonging to the vertical boundaries of the half-plane are set to zero. The displacements of element points are expressed in terms of nodal displacements:

$$U_N = \Phi U \quad . \tag{1}$$

Where $U_N = \begin{bmatrix} U(x,y) \\ V(x,y) \end{bmatrix}$ - the vector of displacements;

$\Phi = \begin{bmatrix} \varphi_1 0 \varphi_2 0 \varphi_3 0 \\ \varphi_1 0 \varphi_2 0 \varphi_3 0 \end{bmatrix}$ - shape matrix;

$\varphi_1, \varphi_2, \varphi_3$ - form functions on an element;

$U=\left[u_{1,}v_{1,}u_{2,}v_{2,}u_{3,}v_{3}\right]^{T}$ - vector of nodal values of displacements on the element.

We carry out a functional expressing the potential energy of a deformed body:

$$I=\sum_{e=1}^{e=l} t_e \int_{\Omega_e} \frac{1}{2}\varepsilon^{T}\sigma\, d\,\Omega_e - \sum_{e=1}^{e=l} t_e \int_{\Gamma_e} U_N{}^{T} Q\, d\,\Gamma_e \quad . \tag{2}$$

Here the contributions are summed over l - elements, each of them with thickness t_e, area Ω_e;

$\varepsilon=(\varepsilon_x,\varepsilon_y,\gamma_{xy})^{T}$ - deformation vector,

$\sigma=(\sigma_x,\sigma_y,\tau_{xy})^{T}$ - stress vector,

$Q=(q_x,q_y)^{T}$ is the vector of the distributed load applied to the boundary Γ_e of the boundary element e.

The relationship between stresses and deformation is expressed by Hooke's law (Timoshenko, J.N. Goodier, 1970):

$$\sigma = D\varepsilon \quad . \tag{3}$$

Here D is the elasticity matrix of the element:

$$D=\frac{E}{1-\nu^{2}}\begin{bmatrix}1 & \nu & 0\\ \nu & 1 & 0\\ 0 & 0 & (1-\nu)/2\end{bmatrix} \quad ,$$

where E is the modulus of deformation on the element,

ν - Poisson's ratio on the element.

The relationship between displacement and deformation is expressed by the formula (Timoshenko and Goodier, 1970):

490
$$\varepsilon = \begin{bmatrix} \dfrac{\partial u}{\partial x} \\ \dfrac{\partial v}{\partial y} \\ \dfrac{\partial u}{\partial x} + \dfrac{\partial v}{\partial y} \end{bmatrix}$$

491 or, taking into account (1), we write

$$\varepsilon = B \cdot U \tag{4}$$

492 where

493
$$B = \begin{bmatrix} \dfrac{\partial}{\partial x} & 0 \\ 0 & \dfrac{\partial}{\partial y} \\ \dfrac{\partial}{\partial x} + \dfrac{\partial}{\partial y} \end{bmatrix} \cdot \Phi = \begin{bmatrix} \dfrac{\partial \varphi_1}{\partial x} & 0 & \dfrac{\partial \varphi_2}{\partial x} & 0 & \dfrac{\partial \varphi_3}{\partial x} & 0 \\ 0 & \dfrac{\partial \varphi_1}{\partial y} & 0 & \dfrac{\partial \varphi_2}{\partial y} & 0 & \dfrac{\partial \varphi_3}{\partial x} \\ \dfrac{\partial \varphi_1}{\partial y} & \dfrac{\partial \varphi_1}{\partial x} & \dfrac{\partial \varphi_2}{\partial y} & \dfrac{\partial \varphi_2}{\partial x} & \dfrac{\partial \varphi_3}{\partial y} & \dfrac{\partial \varphi_3}{\partial x} \end{bmatrix} .$$

494 We accept the functions of the shape of the element as linear and equal on the element to its

495 barycentric coordinates, and outside the element to zero:

496
$$\varphi_i = \frac{a_i x + b_i y + c_i}{2S}, i = 1,2,3 \quad .$$

497 Where S is the area of the element,

$$\left.\begin{array}{l} a_1 = y_2 - y_3 \\ b_1 = x_3 - x_2 \\ c_1 = x_2 y_3 - x_3 y_2 \end{array}\right\} \quad . \tag{5}$$

498

499 The coefficients $a_2, a_3, b_2, b_3, c_2, c_3$ are determined through the cyclic permutation of the indices

500 in (5).

501 Then the matrix B will take the form:

502 $$B=\frac{1}{2S}\begin{bmatrix} a_1\,0\,a_2\,0\,a_3\,0 \\ 0\;b_1\,0\;\;b_2\,0\,b_3 \\ b_1\,a_1\,b_2\,a_2\,b_3\,a_3 \end{bmatrix} \quad .$$

503 Let's rewrite (2) taking into account (1), (3), (4):

$$I=\sum_{e=1}^{e=l} t_e \int_{\Omega_e} \frac{1}{2} U^T B^T D\cdot B\cdot U \, d\Omega_e - \sum_{e=1}^{e=l} t_e \int_{\Gamma_e} U^T \Phi Q \, d\Gamma_e \quad . \qquad (6)$$

504

505 A finite-element solution provides a minimum to functional (6) on the class of functions from a

506 finite-dimensional space with a basis $(\varphi_e)_{e=1}^{e=l}$, $\varphi_e=(\varphi_1^e,\varphi_2^e,\varphi_3^e)$ (Ciarlet, 1978).

507 The necessary condition for the minimum of functional (6):

508 $$\sum_{e=1}^{e=l} \frac{\partial I^e}{\partial U} = \sum_{e=1}^{e=l} \int_{\Omega_e} t_e B^T D\cdot B\cdot U \, d\Omega_e - \sum_{e=1}^{e=l} \int_{\Gamma_e} t_e \Phi Q \, d\Gamma_e = 0, \quad e=1,2,\ldots,l \quad .$$

509 Therefore, we find the solution from the system of linear equations:

$$K_f\cdot U_f = F_f \quad . \qquad (7)$$

510

511 Here U_f is the global vector of nodal values:

512 $$U_f=(U^1,U^2,\ldots,U^l)^T \quad ,$$

513 K_f - a global stiffness matrix composed of element stiffness matrices (the so-called local

514 stiffness matrices) K^e :

515 $$K^e=\int_{\Omega_e} t_e B^T D B U \, d\Omega_e \quad ,$$

516 F_f - global load vector, composed of load vectors of elements:

517 $$F_f^e=\int_{\Gamma_e} t_e \Phi^T Q \, d\Gamma_e \quad .$$

518 Consider a boundary element with a distributed vertical load applied to it (Figure 3.3).

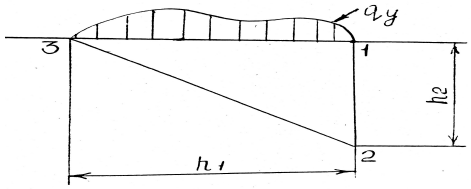

Figure 3.3 Scheme of load application to the boundary element.

520 In the case of linear linear functions of the form, we have on the boundary:

521 $$\varphi_2 = 1 - \frac{s}{h_1} \quad , \quad \varphi_3 = \frac{s}{h_1}$$

522

$$F_f^e = t_e \int_0^{h_1} (0 \;\; 0 \;\; 0 \;\; \varphi_2 q_y \;\; 0 \;\; \varphi_3 q_y)^T \, dS \quad . \tag{8}$$

523

524 Here are the specific values of the matrices and coefficients. Let's denote for convenience

525 $$\xi = \frac{h_1}{h_2} \quad .$$

526 The matrix B^e

527 Elements of the 1st type

528 $$B^{(1)} = \begin{bmatrix} 0 & 0 & -1/\xi & 0 & 1/\xi & 0 \\ 0 & \xi & 0 & -\xi & 0 & 0 \\ \xi & 0 & -\xi & -1/\xi & 0 & 1/\xi \end{bmatrix}$$

529

530

Elements of the 2nd type

$$B^{(2)}=\begin{bmatrix} 0 & 0 & 1/\xi & 0 & -1/\xi & 0 \\ 0 & -\xi & 0 & \xi & 0 & 0 \\ -xi & 0 & \xi & 1/\xi & 0 & -1/\xi \end{bmatrix}$$

Elements of the 3rd type

$$B^{(3)}=\begin{bmatrix} -1/\xi & 0 & 0 & 0 & 1/\xi & 0 \\ 0 & \xi & 0 & -\xi & 0 & 0 \\ \xi & -1/\xi & -xi & 0 & 0 & 1/\xi \end{bmatrix}$$

Elements of the 4th type

$$B^{(4)}=\begin{bmatrix} 1/\xi & 0 & 0 & 0 & -1/\xi & 0 \\ 0 & -\xi & 0 & \xi & 0 & 0 \\ -xi & 1/\xi & xi & 0 & 0 & -1/\xi \end{bmatrix} .$$

The Matrix K^e

We denote $d=\dfrac{1-\nu}{2}$

Elements of the 1st type

$$\frac{E}{2(1-\nu^2)}\begin{bmatrix} \xi d & 0 & -\xi d & -d & 0 & d \\ 0 & \xi & -\nu & -\xi & \nu & 0 \\ -\xi d & -\nu & 1/\xi+\xi d & \nu+d & -1/\xi & -d \end{bmatrix}$$

Elements of the 2nd type

$$\frac{E}{2(1-\nu^2)}\begin{bmatrix} -d & -\xi & \nu+d & \xi+d/\xi & -\nu & -d/\xi \\ 0 & \nu & -1/\xi & -\nu & 1/\xi & 0 \\ d & 0 & -d & -d/\xi & 0 & d/\xi \end{bmatrix}$$

Elements of the 3rd type

$$\frac{E}{2(1-\nu^2)}\begin{bmatrix} 1/\xi+\xi d & -\nu-d & -\xi d & \nu & -1/\xi & d \\ -\nu-d & \xi+d/\xi & d & -\xi & \nu & -d/\xi \\ -\xi d & d & \xi d & 0 & 0 & -d \end{bmatrix}$$

545

546 Elements of the 4th type

547 $$\frac{E}{2(1-\nu^2)}\begin{bmatrix} \nu & -\xi & 0 & \xi & -\nu & 0 \\ -1/\xi & \nu & 0 & -\nu & 1/\xi & 0 \\ d & -d/\xi & -d & 0 & 0 & d/\xi \end{bmatrix} .$$

548 The matrix K_f of the system (7) is composed of the stiffness matrices of the elements K^e in
549 the following way. Suppose there are l -elements (Figure 3.1), we number all the vertices from
550 left to right and from top to bottom. The matrix K_f has a dimension of $2\cdot l\times 2\cdot l$. Let's
551 imagine it consisting of blocks (2x2). The dimension of such a matrix will be $l\times l$. Matrices of
552 elements, as block ones, consisting of 2x2 submatrices, have a dimension of 3x3. Let the vertices
553 of the elements belonging to the upper layer have numbers i and (or) $i+1$, and the vertices
554 of the elements belonging to the lower layer have numbers j and (or) $j+1$. Then the
555 following contribution to K_f will be made:

556 elements of the 1st type

557 $$K_f(j,j)=K_f(j,j)+KL(1,1)$$

558 ($KL(1,1)$ - are the corresponding submatrices (2x2) of the matrix $K^{(1)}$)

559
$$\begin{aligned} &K_f(i,i)=K_f(i,i)+KL(2,2) \\ &K_f(i+1,i+1)=K_f(i+1,i+1)+KL(3,3) \\ &K_f(j,i)=K_f(j,i)+KL(1,2) \\ &K_f(j,i+1)=K_f(j,i+1)+KL(1,3) \\ &K_f(i+1,i)=K_f(i+1,i)+KL(3,2) \end{aligned}$$

560

561

562

elements of the 2nd type

$$
\begin{gathered}
K_f(i+1,i+1)=K_f(i+1,i+1)+KL(1,1) \\
K_f(j+1,j+1)=K_f(j+1,j+1)+KL(2,2) \\
K_f(j,j)=K_f(j,j)+KL(3,3) \\
K_f(j+1,i+1)=K_f(j+1,i+1)+KL(2,1) \\
K_f(j+1,j)=K_f(j+1,j)+KL(2,3) \\
K_f(j,i+1)=K_f(j,i+1)+KL(3,1)
\end{gathered}
$$

elements of the 3rd type

$$
\begin{gathered}
K_f(j,j)=K_f(j,j)+KL(1,1) \\
K_f(i,i)=K_f(i,i)+KL(2,2) \\
K_f(j+1,j+1)=K_f(j+1,j+1)+KL(3,3) \\
K_f(j,i)=K_f(j,i)+KL(1,2) \\
K_f(j+1,j)=K_f(j+1,j)+KL(3,1) \\
K_f(j+1,i)=K_f(j+1,i)+KL(3,2)
\end{gathered}
$$

elements of the 4th type

$$
\begin{gathered}
K_f(i+1,i+1)=K_f(i+1,i+1)+KL(1,1) \\
K_f(j+1,j+1)=K_f(j+1,j+1)+KL(2,2) \\
K_f(i,i)=K_f(i,i)+KL(3,3) \\
K_f(i+1,i)=K_f(i+1,i)+KL(1,3) \\
K_f(j+1,i+1)=K_f(j+1,i+1)+KL(2,1) \\
K_f(j+1,i)=K_f(j+1,i)+KL(2,3)
\end{gathered}
$$

It is known from finite element theory (Ciarlet, 1978) that the matrix K_f is symmetric and positive definite. Therefore, the filling of elements lying only on the main diagonal and below is shown. Next, we destroy the rows and columns of the matrix corresponding to the nodes (vertices) lying on the border of the selected area (except for the zero horizontal).

In the case of modeling the impact of a load on a soil layer lying on a very weak foundation (eg swamp), we do not impose restrictions on the lower boundary.

The contribution to the global load vector F_f - the right-hand side of system (7) is determined from each element by formula (8). In this case, the node with the number t corresponds to the

$(2t-1)$ and $2t$ lines of the vector F_f . Lines corresponding to border nodes are destroyed.

After finding the nodal displacements, the value of the stresses that are constant on the element is determined by the formula (3). The values of the stresses at the nodes are found by averaging over neighboring elements.

Stress matrix σ

$$\sigma=\begin{bmatrix}\sigma_x\\ \sigma_z\\ \tau_{xy}\end{bmatrix} .$$

Let's introduce the notation:

$$K_\sigma=\frac{E}{(1-\nu^2)h_1h_2} \quad ; \quad \alpha=\frac{1-\nu}{2} \quad ;$$

$$u_{12}=u_1-u_{2,}\ u_{13}=u_1-u_{3,}\ u_{23}=u_2-u_{3,}$$
$$v_{12}=v_1-v_{2,}\ v_{13}=v_1-v_{3,}\ v_{23}=v_2-v_3 .$$

Elements of the 1st type

$$\sigma=K_\sigma\begin{bmatrix}-h_2u_{23}+\nu h_1v_{12}\\ -\nu h_2u_{23}+h_1v_{12}\\ \alpha[h_1u_{12}-h_2v_{23}]\end{bmatrix}$$

Elements of the 2nd type

$$\sigma=K_\sigma\begin{bmatrix}h_2u_{23}-\nu h_1v_{12}\\ \nu h_2u_{23}-h_1v_{12}\\ -\alpha[h_1u_{12}+h_2v_{23}]\end{bmatrix}$$

Elements of the 3rd type

$$\sigma = K_\sigma \begin{bmatrix} -h_2 u_{13} + \nu h_1 v_{12} \\ -\nu h_2 u_{13} + h_1 v_{12} \\ \alpha [h_1 u_{12} - h_2 v_{13}] \end{bmatrix}$$

Elements of the 4th type

$$\sigma = K_\sigma \begin{bmatrix} h_2 u_{13} - \nu h_1 v_{12} \\ \nu h_2 u_{13} - h_1 v_{12} \\ -\alpha [h_1 u_{12} + h_2 v_{13}] \end{bmatrix} .$$

Further, according to the formulas of section (2), we determine the initial values of pressures, heads and stresses.

4. Software implementation and calculation results

4.1 Main software modules

MKESol – main module;

UnCode - contains subroutines for identifying the area of the partition;

SplinUnt - contains subroutines for constructing an interpolation cubic spline and for outputting spline values at specified points;

GetSpline - the procedure for forming the global load vector (the right side of the linear algebraic system of equations);

GetData - procedure for generating a global stiffness matrix;

LDL - contains routines for decomposition and solutions for strip matrices by the Cholesky

613 method (Reinsch and Wilkinson, 1971).

614 After the soil program has been processed, the values of the grid functions from the space V
615 that define the vertical and horizontal displacements are known. These values are recorded in the
616 Output.mke file;

617 MKEDrow - control module for presenting calculation results;

618 Sigma - contains programs for calculating mesh functions from a subspace $U_{1,}\ldots, U_{s}$. The
619 initial data is the values of the mesh displacement functions contained in the Output.mke file;

620 FuncLoad - contains numerical integration routines for finding a solution to the first boundary
621 value problem in the case of an isotropic medium;

622 Anal - contains subroutines for graphical representation of a grid function in the form of function
623 level lines of two variables. This representation is performed by the LineLab (Nf, k) procedure.
624 Here Nf is a parameter defining the identifier code of the grid function; k is the number of level
625 lines on the display screen.

626

Nf	Level line
0	σ_x - steady-state stresses along the axis x, kg/cm^2
1	σ_z - steady-state stresses along the axis z, kg/cm^2
2	τ_{xz} - steady-state shear stresses along the axis x, kg/cm^2
3	σ_{xo} - initial stresses along the axis x, kg/cm^2
4	σ_{zo} - initial stresses along the axis z, kg/cm^2
5	P_o - initial pressures, kg/cm^2
6	V - vertical deformations, cm
7	Θ_{max} - the maximum angle of deviation of the full stress vector, $grad$
Encoding for solving the First Boundary Value Problem (FuncLoad module)	
10	σ_{xo} - initial stresses along the axis x, kg/cm^2
11	σ_{zo} - initial stresses along the axis z, kg/cm^2
12	P_o - initial pressures, kg/cm^2

Nf encoding table.

4.2 Calculation results

The figures 4.1 - 4.4 show the results of calculating the zones of vertical stresses from the impact of the ML-56 machine for different types of tires:

33L-32F134;

33L-32F134M - with reduced pressure;

71x47-25; 79x59-26} ultra wide-profile.

Movement on loamy soil is simulated. The soil is presented in two layers: a thin layer of 30 cm on a denser base. The relative humidity of the soil is 80%. The characteristics of the soil are presented in the table 4.1.

	Deformation modulus E, kg/cm^2	Poisson's ratio ν	Internal grip C_o, kg/cm^2	Internal friction angle φ_o, $grad.$
Upper layer	100	0,3	0,21	15
Bottom layer	370	0,3	0,60	18

Table 4.1 Soil characteristics.

636 An intensive increase in rutting can be expected during trips by the machine with 33L-32F134
637 tires as a result of vertical deformation in the soil and lateral uplift caused by the movement of
638 destroyed soil into zones with zero and negative (i.e. tensile) vertical stresses. This is the
639 manifestation of the flat phenomena of the mathematical model.

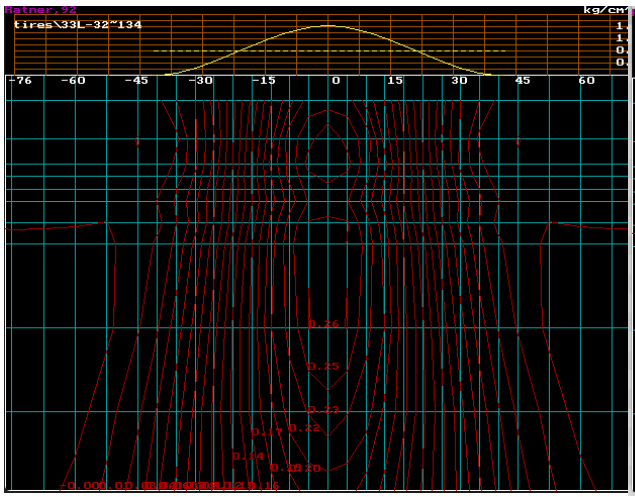

Figure 4.1 Distribution of initial stresses $\sigma_{zo}, kg/cm^2$. Tires 33L-32FI34.

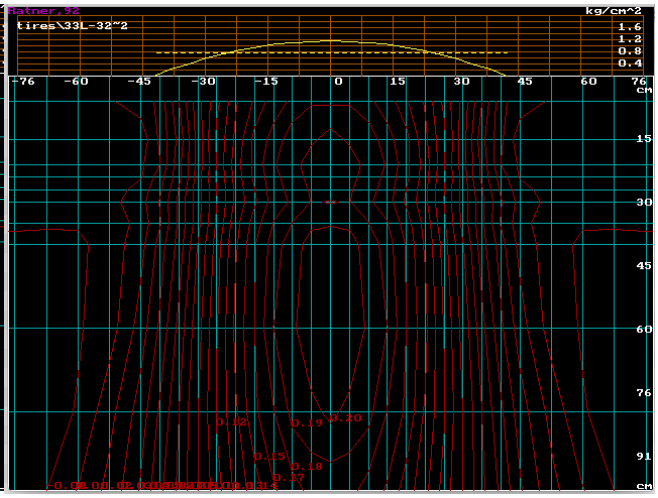

Figure 4.2 Distribution of initial stresses $\sigma_{zo}, kg/cm^2$. Tires 33L-32FI34 M.

Comparing the figures 4.1 and 4.2, we can note the absence of soil zones with a destroyed structure (Figure 4.2) in the case of using the 33L-32F134 M tire with an internal air pressure of 0.8 kg / cm ^ 2. This is due to a change in the shape of the loading diagram with a decrease in the internal air pressure from 1.4 to 0.8 kg / cm ^ 2.

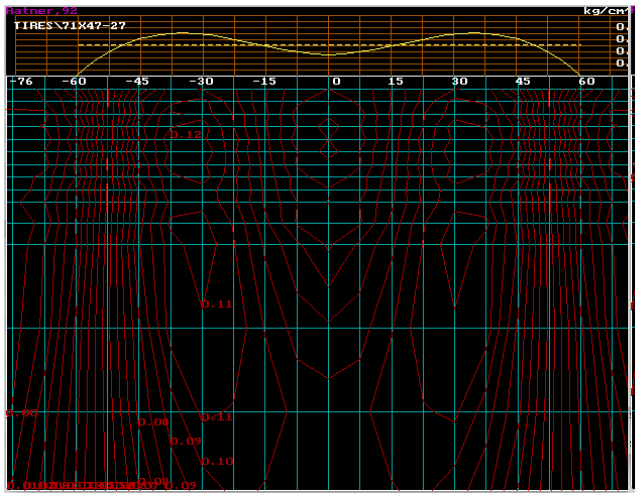

Figure 4.3 Distribution of initial stresses $\sigma_{zo}, kg/cm^2$ *. Tires 71x47-25.*

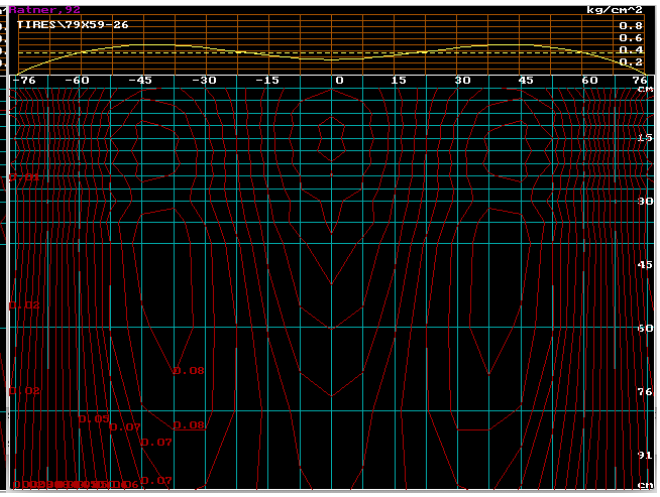

Figure 4.4 Distribution of initial stresses $\sigma_{zo}, kg/cm^2$ *. Tires 79x59-26.*

5. Experimental data

The figures 5.1 – 5.4 show the calculated zones of vertical stresses from the impact of the TT-4M tractor with a highly elastic and serial track. The soil is homogeneous (in modulus of deformation), therefore, an analytical solution to the first boundary value problem is presented. The characteristics of the soil are presented in table 5.1. Available experimental data (mean values of pressure sensors over time series) are presented in Table 5.2 (Ratnere, 1993).

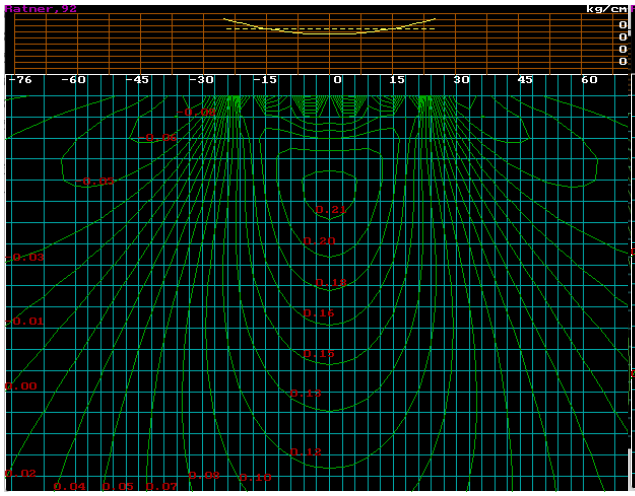

Figure 5.1 Distribution of initial stresses $\sigma_{zo}, kg/cm^2$ *in a homogeneous medium. Serial track.*

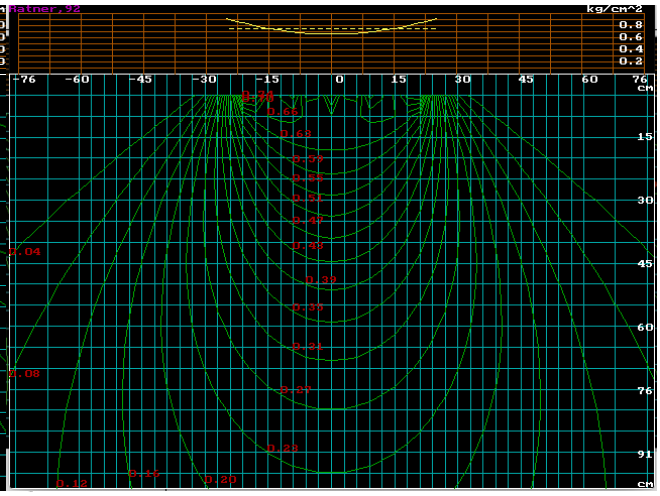

Figure 5.2 Distribution of steady-state stresses $\sigma_z, kg/cm^2$ *in a homogeneous medium. Serial track.*

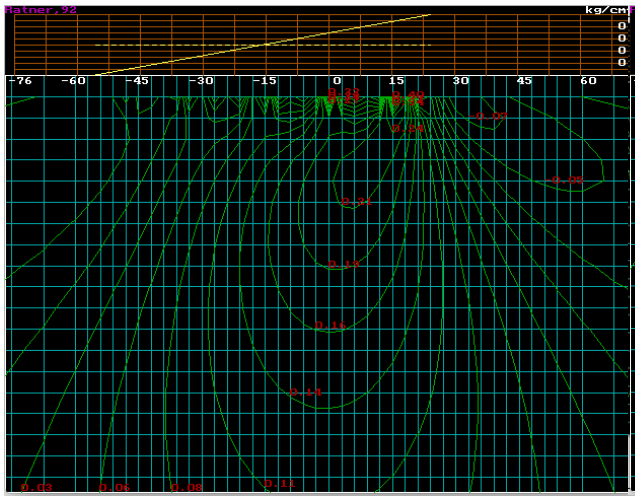

Figure 5.3 Distribution of initial stresses $\sigma_{zo}, kg/cm^2$ *in a homogeneous medium. Highly elastic track.*

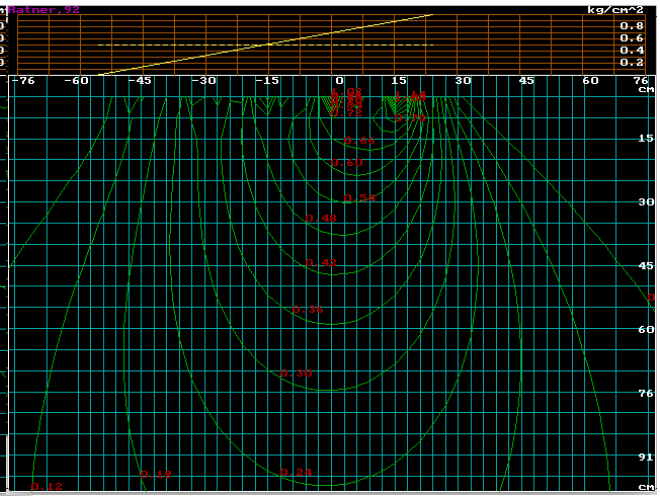

Figure 5.4 Distribution of steady-state stresses $\sigma_z, kg/cm^2$ *in a homogeneous medium. Highly elastic track.*

Sampling depth, cm	The number of strikes by the a striker	Soil deformation modulus for a striker, MPA	Density of wet soil g/cm^3	Density of the soil skeleton g/cm^3
20	3.33	5.0	2.04	1.7
40	4.0	6.0	2.02	1.68
60	2.75	4.12	2.11	1.74

Table 5.1 Physical and mechanical indicators of soils and grounds on measured plots.

648

Distance from the center of the treadmill to the pressure sensors, cm			
	-25	0	25
Serial track. Gross weight of the tractor 21250 kg			
Top row	0.090	0.384	...
+ 20 см	0.196	0.333	0.357
+ 40 см	...	0.231	...
Highly elastic track. Gross weight of the tractor 23900 kg			
Top row	0.060	...	1.538
+ 20 см	0.190	0.282	0.289
+ 40 см	...	0.189	...

Table 5.2 Average values of pressures, kg/cm^2 .

649 It can be seen from Table 5.2 that the general view of the calculated distribution functions of
650 vertical stresses for both types of tracks is in good agreement with the experimental data. The
651 experimental values of stresses are greater than the initial calculated values, but less than the
652 steady-state values of stresses. This can be explained by the following factors:

653 a) The initial distance from the top layer of the sensors (20 cm) decreased as a result of soil

deformation.

b) The values of pressures averaged over the time series are taken as experimental data, i.e. pressure from the load, which acts for some time, and the initial stresses from the instantly applied load are taken as the calculated ones, the value of which is averaged over the reference area of the track.

c) Pressure sensors perceive the load, the components of which are the load from water pressure and the load from vertical stresses in the soil skeleton, and we calculate only vertical stresses in the skeleton.

Conclusion

The presented mathematical model, together with its software implementation, makes it possible to assess the degree of influence of the tire of a forest wheeled tractor on the waterlogged forest soil, depending on the design parameters of the tire and the vertical loads that fall on it.

The adequacy of the mathematical model is confirmed by the conducted experimental studies, as well as by numerous test results of forest wheeled tractors.

The model is developed based on the theory of soil mechanics. The plane problem of compaction of water-saturated anisotropic (in the general case) soil is considered. It was shown that with an instantaneous application of a vertical load, the initial distribution of stress and water pressure in the soil are expressed through their values in a state of complete stabilization. Therefore, it is conventionally assumed that the magnitude of the load does not change before the onset of this state, causing linear (relative to the load) deformations of the soil.

Thus, first, a plane problem of different modulus of the theory of a linearly deformable medium is solved. This problem is described by a system of partial differential equations (equations 7-9 of section 1). The solution is found by the finite element method with respect to displacements.

Then, the steady-state and initial values of the stresses are determined, as well as the values of the maximum deviation of the total stress vector - θ_{max} .

In the case of an isotropic medium, the initial heads function (H_o) satisfies the Laplace equation: $\Delta H_o = 0$. The first boundary value problem is posed and solved. Analytical expressions are obtained for the initial values of water heads, pressure and stresses. With their help, one can select the optimal triangulation of the region for a given loading diagram and check the finite element solution.

The initial data for this mathematical model are the layer-by-layer values of the deformation modulus, Poisson's ratio, adhesion coefficient C_o , and angle of internal friction φ_o . Condition: $\theta_{max} = \infty$ means that the soil mass is in a state of ultimate plastic equilibrium.

The calculation results are presented as level lines of the function of two variables. The general view of the vertical stress function is in good agreement with the available experimental data.

It was found that the form of the transverse loading diagram has a significant effect on the degree of the stress state of the soil. At the same average contact pressures, the parabolic shape of the loading diagram, which is characteristic of tires with reduced internal air pressure, has the smallest effect on the soil.

The method can serve as the basis for predicting the degree of soil compaction and the intensity of rutting, as well as the environmental consequences of the operation of forest machines.

Acknowledgement

The author sincerely grateful to Mr. Philip Rodriguez for his help in preparing the text.

Computer Code Availability

Name of code: soil-models

Dr. Igor Ratnere, Lawrence Berkeley National Laboratory

1 Cyclotron Road, M/S 91R0183, Berkeley, CA 94720, iratnere@lbl.gov, 510-495-8373 (Office)

Hardware required: Mac (Mac OS) or PC (Windows)

Program language: Turbo Pascal

Software required: DosBox, Turbo Pascal

(https://gist.github.com/nvgrw/da00b5d3ac96b9c45c80)

Program size: 408 KB

The source codes are available for downloading at the link: https://github.com/igorratn/soil-models.git

References

Ciarlet P.G. 1978. The finite element method for elliptic problems, Vol.4. North Holland, 529 pp.

Gersevanov N.M. 1948. Research in the field of soil dynamics, mechanics and applied mathematics. M.: Stroyvoenmorizdat, 376 pp. [in Russian].

Florin V.A. 1954. Fundamentals of Soil Mechanics, Vol.1. M.: Gosstroyizdat, 358 pp. [in Russian].

Florin V.A. 1961. Fundamentals of Soil Mechanics, Vol.2. M.: Gosstroyizdat, 544 pp. [in Russian].

Nikiforov A.F. 1983. Methods of Mathematical Physics. M.: Ed. Moscow State University, 224 pp. [in Russian].

719 Pokrovsky G.I. 1941. Friction and traction in soils. M.: Stroyizdat, 120 pp. [in Russian].
720 Reinsch C. , Wilkinson J.H. 1971. Handbook for Automatic Computation. Berlin, Heidelberg:
721 Springer, 441 pp.
722 Ratnere I.S. 1993. Determination of traction reference indicators of a wheeled forestry tractor
723 and assessment of soil condition parameters. Dissertation for the degree of candidate of technical
724 sciences. Khimki, 215 pp. [in Russian].
725 Terzagi K. 1961. Theory of soil mechanics. M.: Stroyizdat, 508 pp. [in Russian].
726 Timoshenko S.P, Goodier J.N., 1970. Theory of elasticity. Mcgraw-Hill Eduction; 3rd edition,
727 608 pp.
728

List of Figures

753 19. Figure 5.4: Distribution of steady-state stresses σ_z, kg/cm^2 in a homogeneous medium.

754 Highly elastic track.

755